

Transition1x - a Dataset for Building Generalizable Reactive Machine Learning Potentials

Mathias Schreiner¹, Arghya Bhowmik², Tejs Vegge², Jonas Busk², Ole Winther^{1,3,4}

¹ DTU Compute, Technical University of Denmark (DTU)

² DTU Energy, Technical University of Denmark (DTU)

³ Department of Biology, University of Copenhagen (UCph)

⁴ Genomic Medicine, Copenhagen University Hospital, Rigshospitalet

ABSTRACT

Machine Learning (ML) models have, in contrast to their usefulness in molecular dynamics studies, had limited success as surrogate potentials for reaction barrier search. It is due to the scarcity of training data in relevant transition state regions of chemical space. Currently, available datasets for training ML models on small molecular systems almost exclusively contain configurations at or near equilibrium. In this work, we present the dataset Transition1x containing 9.6 million Density Functional Theory (DFT) calculations of forces and energies of molecular configurations on and around reaction pathways at the ω B97x/6-31G(d) level of theory. The data was generated by running Nudged Elastic Band (NEB) calculations with DFT on 10k reactions while saving intermediate calculations. We train state-of-the-art equivariant graph message-passing neural network models on Transition1x and cross-validate on the popular ANI1x and QM9 datasets. We show that ML models cannot learn features in transition-state regions solely by training on hitherto popular benchmark datasets. Transition1x is a new challenging benchmark that will provide an important step towards developing next-generation ML force fields that also work far away from equilibrium configurations and reactive systems.

I. INTRODUCTION

ML for interatomic potentials for molecular systems has in recent years achieved accuracy comparable to quantum mechanical (QM) methods with computational cost of classical interatomic potentials^{10,34,5,3,33}. The development of such data-driven models has ushered in a new age in computational chemistry over the last few years^{30,2,13,7}. ML potentials have been used for structural optimization and studying finite-temperature dynamical properties through molecular dynamics^{14,32}. ML potentials are especially suited for screening through large numbers of molecules or simulating systems that are too large for traditional QM methods due to a complexity scaling that is orders of magnitudes lower. The applicability of models depends on the

sampling of training data of chemical and structural space³¹. Fitting ML models to the entire potential energy surface (PES) requires vast amounts of carefully selected data as the underlying electronic interaction between atoms is of a complex, quantum mechanical nature. Thus the focus remains on an efficient sampling strategy of the useful parts of the PES that are relevant to the application. For example, models for optimization tasks should be trained on datasets including small perturbations to equilibrium geometries, and models for molecular dynamics (MD) simulations and reactive systems should be trained on datasets with geometries from all parts of the PES, including states that represent the making and breaking of bonds.

ML potentials that allow accurate modeling

of reaction barriers are challenging to train and only limited demonstrations have been achieved recently³⁵. Data sets need much larger scale sampling of the higher energy part (compared to near-equilibrium geometry) of the high dimensional PES for models to learn all sections of the transition pathway accurately. The earliest work studying simple diatomic molecule dissociation required tens of thousands of data points to achieve accuracy¹⁸. Related other work to date^{17,35,19} have focused on single or few reactions involving small molecules with tractable data set size. Thus current state-of-the-art ML potentials do not allow high throughput estimation of reaction barriers for thousands of reactions. The development of such models would require massive amounts of training data and complex models that can generalize across numerous PESs of reactive molecule sets. Recently, the development of neural network architectures that learn representation and energy/force mapping³⁰ has tackled the problem of highly expressive models. Data sets that help such models generalize across a large number of reactions remain an open challenge. One approach to building such data sets is to run high-temperature MD simulations of molecules and molecular aggregates²⁸. But this does not provide any guarantees that transition states will be sampled, as often kinetic barriers are large and reaction transitions are rare events.

Sampling of rare events is efficiently done with the NEB method²⁶. Here we propose a new data set for building ML models capable of generalizing across a large variety of reaction PESs. We leverage NEB-based PES exploration as an efficient data collection tool and prove its superiority compared to MD-based dataset preparation by testing the accuracy of ML models built from both types of data.

Ultra-fast prediction of chemical reaction kinetics especially for computational modeling of complex reaction networks is groundbreaking

for the entire field of chemical and molecular sciences. We believe that the Transition1x data set will expedite the development and testing of universal reactive ML potentials that help the community archive that goal.

II. METHODS

Starting from a set of 11961 reactions¹¹ with reactants, transition states, and products, NEB is used to explore millions of molecular configurations in transition-state regions, using DFT to evaluate forces and energies. The resulting DFT calculations are available in the Transition1x dataset. Figure 1 presents an overview of the workflow. Reactant and product are relaxed for any particular reaction before generating an initial path using Image Dependent Pair Potential (IDPP)²⁷. Next, the minimal energy path (MEP) is optimized with NEB²⁶ and consecutively Climbing Image Nudged Elastic Band (CINEB)¹² until convergence. If the path converges, we save the DFT calculations from the iterations where the path moved significantly.

Initial Data

The data generating procedure starts by taking an exhaustive database¹¹ of product-reactant pairs based on the GDB7 dataset²³. The authors of this data used the Growing String Method (GSM)³⁶ with the ω B97X-D3⁶/def2-TZVP level of theory to generate reactants, products, and transition states for 11961 reactions using Qchem⁹.

DFT Potential

For compatibility with ANI1x²⁸, the ω B97x⁶ - a hybrid-meta GGA functional, which is chemically accurate compared to high-level CCSD(T) calculations²¹ and the 6-31G(d)⁸ basis set is applied to perform all calculations in ORCA 5.0.2²⁰.

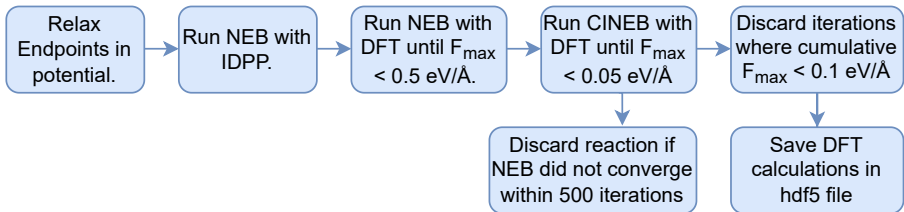


Figure 1: Overview of the data generation workflow. First, reactant and product are relaxed before generating an initial MEP guess with IDPP²⁷. Next NEB²⁶ and CINEB¹² is run on the initial path until convergence. If the MEP does not converge within 500 iterations we discard the reaction, as unphysical configurations may have been encountered. If the reaction converges, all intermediate paths are saved in the dataset, as long as they are sufficiently different from previously saved paths.

Optimizer

The BFGS optimizer⁴ implemented in Atomic Simulation Environment (ASE)¹⁶ with $\alpha = 70$ and a maximal step size of 0.03 \AA is used for all optimization tasks, including relaxing endpoints before NEB and relaxing MEPs with both NEB and CINEB.

Initial Path Generation

Product and reactant geometries are relaxed in the potential before running NEB. The configuration is considered relaxed once the norm of the forces in configurational space is less than a threshold of 0.01 eV\AA^{-1} . After relaxing the endpoints an initial path is proposed, built from two segments – one interpolated from the reactant to the transition state found in the original data, and another interpolated from the transition state to the product. Next, the initial path is minimised with NEB using IDPP²⁷, a potential specifically designed to generate physically realistic reaction paths for NEB at a low computational cost. Finally, the path is proposed as the initial MEP in the DFT potential.

NEB

NEB²⁶ is an algorithm for transition state search that works by iteratively improving an initial guess for the reaction pathway by using information of the PES as calculated by some potential. NEB represents the path as a series of geometries called images but with no

guarantee that the maximal energy image, the transition state, represents the maximal energy along the MEP. CINEB¹² is an improvement to the NEB algorithm as it imposes, as an additional condition to the convergence, that the maximal energy image has to lie at a maximum along the path. It does so by, in each iteration, letting the image with the maximal energy climb freely along the reaction path. Running CINEB from the beginning, however, can interfere with the optimizer and result in slow (or wrong) convergence of the MEP as the climbing image can pull the current path off the target MEP if the paths are not close. Therefore, first, the path is relaxed with regular NEB until the maximal perpendicular force to the MEP is below a threshold of 0.5 eV\AA^{-1} . At this point NEB has usually found the qualitatively correct energy valley, and further optimization only nudges the path slightly while finding the bottom. At this point CINEB is turned on to let the highest energy image climb along the path until it finds an energy maximum. CINEB is run until the path has been relaxed fully and the maximal perpendicular force on the path does not exceed 0.05 eV\AA^{-1} . The spring constant used between images is 0.1 eV\AA^{-2} .

Data selection

When running NEB, unphysical configurations are often encountered in reactions that do not converge. Such images in the data will interfere with model training, and therefore those reactions are discarded entirely. There are 10073

converged reactions in Transition1x. In the final steps of NEB, the molecular geometries of images are similar between each iteration as the images are nudged only slightly close to convergence. Data points should be spread out so that models do not overfit to specific regions of the data. Updated paths are only included in the dataset if they are significantly different from previous ones. The maximal perpendicular force, F_{max} , to the path is a proxy for how much the path moves between iterations. Once the cumulative sum of F_{max} from previous iterations since last included path exceeds 0.1 eV\AA^{-1} the current path is included. This means that often in the first iterations of NEB every path is included, but as we move towards convergence new data points are included at a lower frequency.

Model and Training

To validate the dataset, we train and evaluate PaiNN²⁵ models. PaiNN is an equivariant Message Passing Neural Network (MPNN)¹ model specifically designed to predict properties of molecules and materials. Forces are calculated as the negative gradient of the energy wrt. the Cartesian coordinates of the atoms rather than as a direct output from the model. This ensures consistent forces. We used a cut-off distance of 5 \AA to generate the molecular graph neighborhood, three message-passing steps, and 256 neurons in each hidden layer of the model. The model was trained using the ADAM¹⁵ optimizer and an initial learning rate of 10^{-4} . During training, the learning rate was decreased by 20% if no improvement was seen on training data for 10^4 batches. The loss is a combination of a squared error loss on force and energy. The force error is the Euclidian distance between the predicted and the true force vector divided by the number of atoms in the molecule as otherwise the force term would contribute more to the loss on bigger molecules. We split the datasets such that test and validation data each consist of 5% of the total data where configurations contain all atoms (C, N, O, and H). All chemical formu-

las seen in any split are unique to only that split. Potentially, models can learn fundamental principles from simpler molecules, therefore, all molecules with less than three heavy atom types are kept in the training data. The models are trained on the training data with early stopping on the validation data, and we report the mean and standard deviation of Root Mean Square Error (RMSE) and Mean Average Error (MAE) from the evaluation on test data. The models are trained on ANI1x, Transition1x, QM9x.

QM9 and QM9x

QM9²² consists of 135k small organic molecules with various chemical properties. QM9 is ubiquitous as a benchmark for new QM methods, and in order to enable for direct comparison with Transition1x, all geometries from the QM9 dataset is recalculated with the appropriate level of DFT. Since configurations in the original QM9²² are not relaxed in our potential, there will be forces on some configurations. All recalculated geometries are saved in a dataset that we shall refer to as QM9x.

ANI1x

ANI1x²⁸ is a dataset of off-equilibrium molecular configurations generated by perturbing equilibrium configurations using pseudo molecular dynamics. Data is generated through the Query by Committee (QbC) algorithm, a process for automatic data diversification. In QbC an ensemble (committee) of models is trained on the dataset, and new proposed data is added or rejected from the dataset based on the committees variance of the ensemble predictions. It is assumed data point will not add information to the dataset if the committee agrees. It is cheaper to evaluate the committee on data than running DFT calculations, so it is possible to screen many candidate configurations before calculating force and energy with expensive methods. The dataset is generated by alternating between training models and expanding the dataset. The procedure

resulted in force and energy calculations for approximately 5 million configurations containing C, O, N, and H.

III. DATA RECORDS

All data records are available in a single Hierarchical Data Format (HDF5)²⁹ file; Transition1x.h5, hosted by figshare²⁴. It can be downloaded at [here](https://gitlab.com/matschreiner/T1x) or through the repository <https://gitlab.com/matschreiner/T1x>. The HDF5 file structure is as shown in Figure 2. The parent file has four groups, one group contains all data and the three other groups contain symbolic links to the train, test, and validation data – these are the data splits used in this paper. In each data split group, there is a group for each chemical formula under which there is a subgroup for each reaction with the corresponding atoms. Each reaction has four datasets; the atomic numbers of the reaction, the energies of the configurations, the forces acting on the individual atoms, and the positions of atoms. For a reaction with m atoms where we have saved n images, the *atomic_numbers* dataset will have dimensions $(m,)$, one for each atom. The energy dataset will have dimensions $(n,)$, one energy per configuration. The force and position datasets will have dimensions $(n, m, 3)$ as we need three components of position and force for each of m atoms in n configurations. Under each reaction group, there is a child group for reactant, transition state, and product that follow the same structure as described above with $n = 1$. Products from some reactions are reactants for the next, and they can be linked with a hash value available for each product, transition state, and reactant in the hash dataset. The data has been uploaded to figshare, and there is a git repository with data loaders that can turn the HDF5 file into an ASE database or save the configurations as .xyz files.

IV. TECHNICAL VALIDATION

In figure 3 we show the MEP for a reaction and the convergence of NEB for it. Often the barrier grows initially after turning on the climbing image because we start maximizing the energy in a new degree of freedom. NEB converged on 10073 out of 11961 reactions, and 89 percent of the converged reactions did so within the first 200 iterations. To ensure the cleanliness of the data, we choose to discard all reactions that do not converge – these reactions often contain unphysical structures that do more harm than good as training data.

The perpendicular force drops off rapidly when running NEB and so does the variation in data between iterations, as the path is nudged less between iterations, and new data will be similar towards the final iterations of the algorithm. F_{max} is a proxy for how much the path moves between iterations and once the cumulative F_{max} since the last included path exceeds some threshold, the path is included in the dataset.

The transition states found with NEB correspond to the transition states from the original data with GSM as can be seen in Figure 4. Qualitatively, the barrier energies match, but the NEB energies tend to be shifted higher. Generally, it is easier to describe electron clouds around relaxed configurations than around transition states where bonds are breaking and other complex interactions take place. Therefore, the more complex basis set enables us to relax configurations around transition states further than around equilibrium states which results in lower barrier heights. There are more outliers above the $x = y$ line than below it which indicates that GSM was caught in suboptimal reaction pathways more often than NEB.

Figure 5 displays the distribution of forces on each type of atom in Transition1x compared with ANI1x and QM9. Interestingly, even though geometries in Transition1x are further

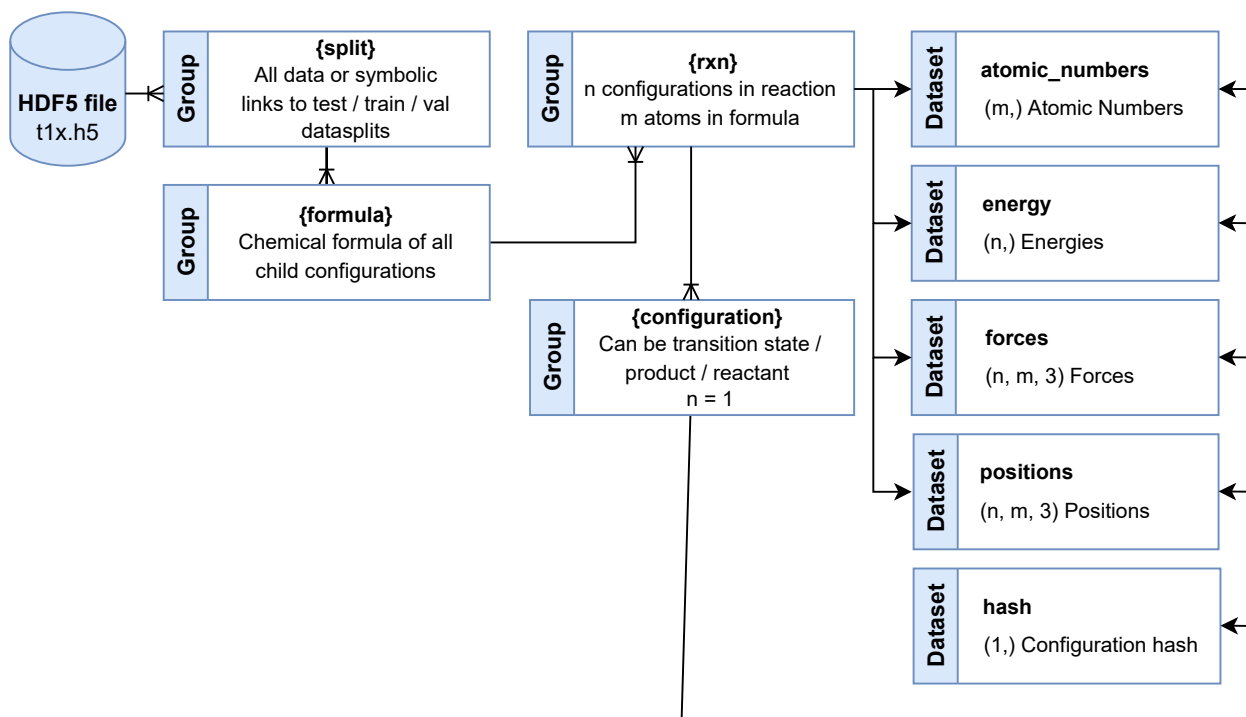


Figure 2: Structure of HDF5 file. Parent groups are data/train/val/test. The data group contains all configurations in the set, and the train/val/test groups contain the suggested data splits used in this paper. Each split has a set of chemical formulas unique to that split, and each formula contains all reactions with the given atoms. Finally, energy and force calculations can be accessed from the reaction groups for all intermediate configurations, including transition-state, product, and reactant.

Trained on	Tested on	Energy [eV]		Forces [eV/Å]	
		RMSE	MAE	RMSE	MAE
ANI1x Transition1x QM9x	Transition States	0.629 (11)	0.495 (10)	0.593 (18)	0.331 (7)
		0.112 (3)	0.075 (1)	0.158 (1)	0.089 (1)
		3.132 (23)	2.957 (25)	0.637 (15)	0.261 (4)
ANI1x Transition1x QM9x	ANI1x	0.044(5)	0.023(1)	0.041(1)	0.016(0)
		0.365(17)	0.226(8)	0.321(25)	0.078(1)
		3.042(13)	2.313(11)	1.314(8)	0.559(2)
ANI1x Transition1x QMx	Transition1x	0.628(63)	0.289(13)	0.542(118)	0.13(5)
		0.102(2)	0.048(1)	0.102(1)	0.046(1)
		2.613(18)	1.421(11)	0.433(3)	0.199(1)
ANI1x Transition1x QM9x	QM9x	0.134(1)	0.124(1)	0.051(1)	0.025(1)
		0.111(2)	0.074(3)	0.072(1)	0.038(0)
		0.04(2)	0.015(1)	0.014(0)	0.005(0)

Table 1: Test results of PaiNN models trained on ANI1x, QM9x, Transition1x. We report RMSE and MAE on energy and forces. Force error is the Euclidian distance between the predicted and true force vector. The test sets have been constructed such that all configurations contain C, N, O, and H, and such that no formula has been seen previously in the training data. We show the best performing model in bold in each test-setup.

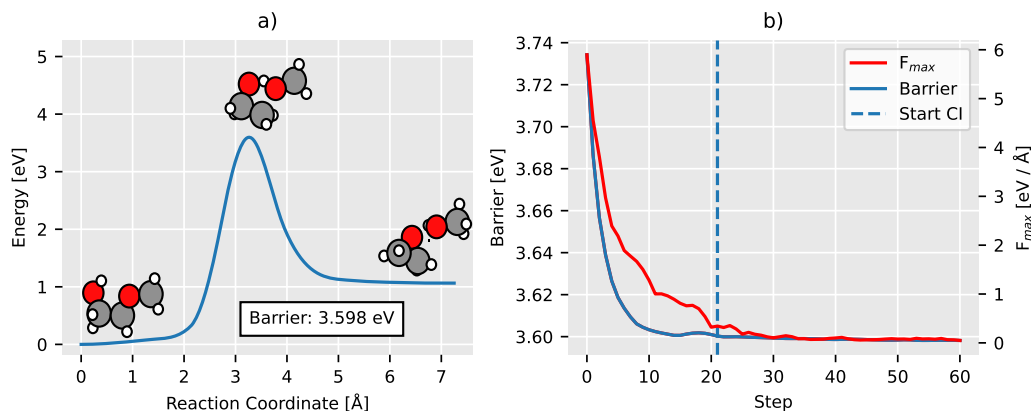


Figure 3: Plot of NEB convergence on example reaction. Panel a) displays the final MEP with reactant, transition state, and product plotted on top with H, C, and O in white, black, and red, respectively. On the x-axis; the reaction coordinate – distance along the reaction path in configurational space, measured in Å. On the y-axis; the difference in potential energy between reactant and current configuration. Panel b) displays the convergence of NEB. On the x-axis; iterations of NEB. On the y-axis; force in $\text{eV}\text{\AA}^{-1}$ and energy barrier in eV at the current step. F_{max} , shown in red, is the maximal perpendicular force acting on any geometry along the path, and Barrier, shown in blue, is the height of the energy barrier found at the current step. Moving right in the plot both F_{max} converges towards zero as NEB finds the saddle point, and the Barrier converges towards the final value of 3.6 eV that can be seen in panel a.

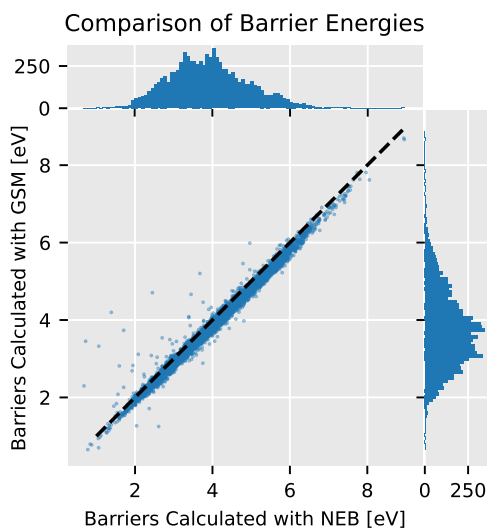


Figure 4: Plot of original barriers versus barriers found in this work. On the x-axis; energies in eV for all transition states calculated using NEB and the 6-31G(d)⁸ basis set. On the y-axis; energies in eV for the corresponding reactions found in¹¹ calculated with GSM and the def2-mSVP basis set.

away from equilibrium than in ANI1x (regions between equilibria are actively sought out in Transition1x), the distribution of forces on ANI1x has flatter, wider tails signifying higher variance in forces. Moreover, Transition1x cusps at zero whereas ANI1x maxima lie further out. Large forces are not necessarily involved when dealing with reactive systems. In fact, when reaction pathways are minimized, forces are minimized too in all but one degree of freedom. The transition states contribute as much to the force distribution as equilibrium configurations, as the transition state is a saddle point with no net force on any atoms. ANI1x has no inherent bias towards low forces on geometries as it explores configurational space with pseudo-MD and therefore, even though the configurations are closer to equilibrium we see higher variance in forces. On the heavy atoms, the tails are qualitatively equal between ANI1x and Transition1x, trailing off exponentially, but it is different for hydrogen. In ANI1x, forces on Hydrogen trails off exponentially as with the other

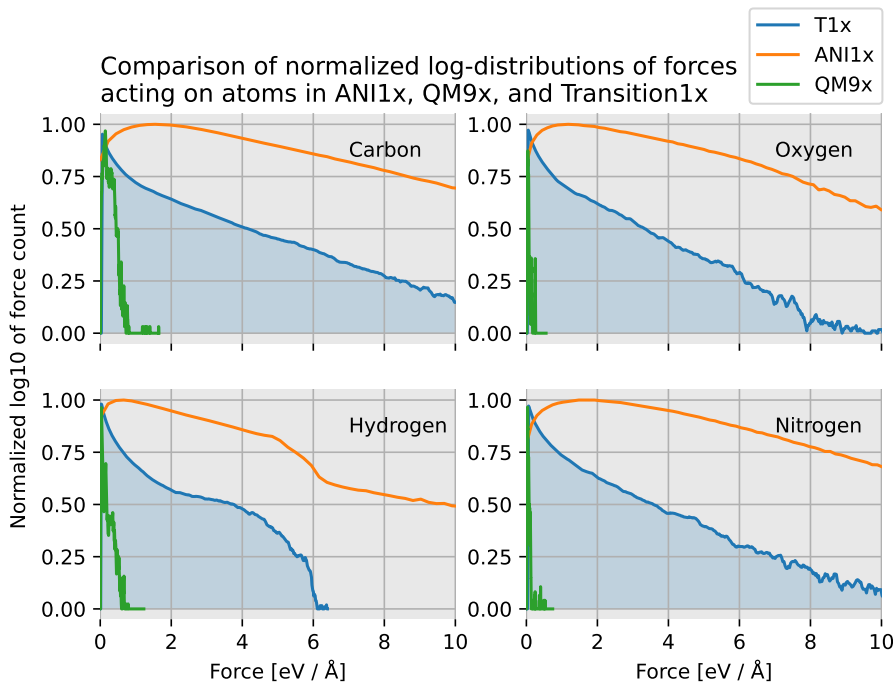


Figure 5: Distribution of forces acting on atom-types in each dataset. The x-axis is the force measured in $\text{eV}/\text{\AA}$. The y-axis is the base 10 logarithm of the count of forces in each bin, normalized over the full domain so that all sets can be compared. In blue; Transition1x. In yellow; ANI1x. In green QM9x.

atoms, but for Transition1x there is a sudden drop of the distribution. Hydrogen atoms are often at the outskirts of the molecules and are relatively free to move compared to heavier atoms on the backbone. In the case of Transition1x data generation procedure, we are minimising energy and forces, and therefore Hydrogen atoms do not experience large forces as they have lots of freedom to relax in the geometry. In ANI1x, configurations are generated by perturbing the geometries randomly, and hydrogen atoms might end up with unrealistically large forces on them. This might be a general problem with ANI1x and also a reason for why ANI1x is not a proper dataset to learn reaction mechanisms.

Even though ANI1x has a wider distribution of forces, the inter-atomic distances between pairs of heavy atoms are less varied than in Transition1x. Figure 6 displays the distribution of distances between pairs of heavy atoms

for Transition1x, ANI1x and QM9. For QM9, a set of only equilibrium configurations, there are some inter-atomic distances that are not present at all. Distances are measured in units of r_0 , the single bond equilibrium distance between the atoms in the smallest possible molecule constructed out of the two. For example, in the case of "C, C" we measure in units of distance between carbon atoms in ethane. Many of the more extreme inter-atomic distances in Transition1x are difficult to produce by normal mode sampling technique of ANI1x as many atoms would randomly have to move such that the whole molecule move along a low-energy valley. However, because NEB samples low-energy valleys by design, we discover likely molecules with inter-atomic distances that are otherwise energetically unfavorable.

We test all resulting models against the test data from each dataset and Transition States

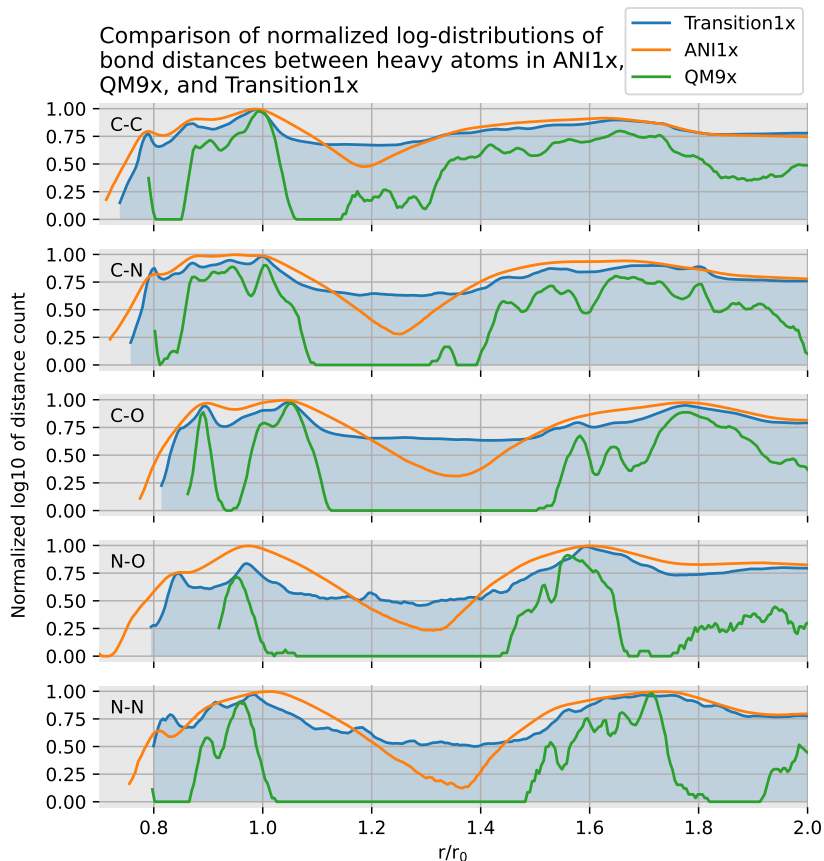


Figure 6: Distribution of interatomic distances between heavy atoms in each dataset. A configuration with n heavy atoms contributes with $n(n-1)/2$ distances in the count. On the y-axis; the log frequency of interatomic distance, normalized between 0 and 1 for comparison as datasets vary in size. On the x-axis; distance given in units of r_0 where r_0 is the equilibrium bond length for a single bond between the smallest possible stable molecule that can be made with the atoms in question. In blue; Transition1x. In yellow; ANI1x. In green; QM9x, recalculated using our level of theory.

from the test reactions. Table 1 displays the results. It is clear from their poor evaluation of Transition1x and transition states, that models trained on ANI1x do not have sufficient data in transition state regions to properly learn the complex interactions present here. ANI1x has a broad variety of chemical structures, but many of the fundamental interactions found in ANI1x are present in Transition1x, which is why models trained on Transition1x perform better on ANI1x than vice versa. In general, the PES of a set of atoms is an incredibly complex function of quantum

mechanical nature. Models trained on QM9x do not perform well on either Transition1x or ANI1x. This is as expected as QM9x contains only equilibrium (or very close to equilibrium in the new potential) structures, so the models trained on it have not seen any of the out-of-equilibrium interactions that are present in the more challenging datasets of ANI1x and Transition1x.

Transition state data is required if we want to replace DFT with cheap ML potentials in algorithms such as NEB or GSM, or train molecular

dynamics models to work in transition state regions. Neural Networks (NNs) are phenomenal function approximators, given sufficient training examples, but they do not extrapolate well. Training examples spanning the whole energy surface are needed to train reliable and general-purpose ML models. Transition1x is a new type of dataset that explores different regions of chemical space than other popular datasets and it is highly relevant as it expands on the completeness of available data in the literature.

V. USAGE NOTES

There are examples and data loaders available in the repository [<https://gitlab.com/matschreiner/T1x>]. There are scripts for downloading the data in HDF5 format and easy-to-use dataloaders that

can loop through the dataset given only the hdf5-path. See repository and documentation for examples of how to use the data loaders and download the dataset.

ACKNOWLEDGEMENTS

The authors acknowledge support from the Novo Nordisk Foundation (SURE, NNF19OC0057822) and the European Union’s Horizon 2020 research and innovation program under Grant Agreement No. 957189 (BIG-MAP) and No. 957213 (BATTERY2030PLUS).

Ole Winther also receives support from Novo Nordisk Foundation through the Center for Basic Machine Learning Research in Life Science (NNF20OC0062606) and the Pioneer Centre for AI, DNRF grant number P1.

REFERENCES

- [1] D. Bacciu, F. Errica, A. Micheli, and M. Podda. A gentle introduction to deep learning for graphs. *Neural Networks*, 129:203–221, 12 2019. doi: 10.1016/j.neunet.2020.06.006. URL <http://arxiv.org/abs/1912.12693><http://dx.doi.org/10.1016/j.neunet.2020.06.006>.
- [2] J. Behler. Four generations of high-dimensional neural network potentials. *Chemical Reviews*, 121(16):10037–10072, 2021.
- [3] J. Behler and M. Parrinello. Generalized neural-network representation of high-dimensional potential-energy surfaces. *Physical review letters*, 98(14):146401, 2007.
- [4] C. G. Broyden. The convergence of a class of double-rank minimization algorithms 1. general considerations. *IMA Journal of Applied Mathematics*, 6:76–90, 3 1970. ISSN 0272-4960. doi: 10.1093/IMAMAT/6.1.76. URL <https://academic.oup.com/imamat/article/6/1/76/746016>.
- [5] S. I. Campbell, D. B. Allan, and A. M. Barbour. Machine learning for the solution of the schrödinger equation. *Machine Learning: Science and Technology*, 1:013002, 4 2020. ISSN 2632-2153. doi: 10.1088/2632-2153/AB7D30. URL <https://iopscience.iop.org/article/10.1088/2632-2153/ab7d30><https://iopscience.iop.org/article/10.1088/2632-2153/ab7d30/meta>.
- [6] J. D. Chai and M. Head-Gordon. Systematic optimization of long-range corrected hybrid density functionals. *The Journal of Chemical Physics*, 128:084106, 2 2008. ISSN 0021-9606. doi: 10.1063/1.2834918. URL <https://aip.scitation.org/doi/abs/10.1063/1.2834918>.
- [7] V. L. Deringer, A. P. Bartók, N. Bernstein, D. M. Wilkins, M. Ceriotti, and G. Csányi. Gaussian process regression for materials and molecules. *Chemical Reviews*, 121(16):10073–10141, 2021.
- [8] R. Ditchfield, W. J. Hehre, and J. A. Pople. Self-consistent molecular-orbital methods. ix. an extended gaussian-type basis for molecular-orbital studies of organic molecules. *The Journal of Chemical Physics*, 54:724, 9 2003. ISSN 0021-9606. doi: 10.1063/1.1674902. URL <https://aip.scitation.org/doi/abs/10.1063/1.1674902>.
- [9] E. Epifanovsky and A. I. Krylov. Software for the frontiers of quantum chemistry: An overview of developments in the q-chem 5 package. *The Journal of Chemical Physics*, 155: 084801, 8 2021. ISSN 0021-9606. doi: 10.1063/5.0055522. URL <https://aip.scitation.org/doi/abs/10.1063/5.0055522>.
- [10] F. A. Faber, L. Hutchison, B. Huang, J. Gilmer, S. S. Schoenholz, G. E. Dahl, O. Vinyals, S. Kearnes, P. F. Riley, and O. A. V. Lilienfeld. Prediction errors of molecular machine learning models lower than hybrid dft error. *Journal of Chemical Theory and Computation*, 13:5255–5264, 11 2017. ISSN 15499626. doi: 10.1021/ACS.JCTC.7B00577/SUPPL_FILE/CT7B00577_SI_001.PDF. URL <https://pubs.acs.org/doi/abs/10.1021/acs.jctc.7b00577>.
- [11] C. A. Grambow, L. Pattanaik, and W. H. Green. Reactants, products, and transition states of elementary chemical reactions based on quantum chemistry. *Scientific Data*, 7, 12 2020. ISSN 20524463. doi: 10.1038/s41597-020-0460-4.
- [12] G. Henkelman, B. P. Uberuaga, and H. Jónsson. A climbing image nudged elastic band method for finding saddle points and minimum energy paths. *The Journal of Chemical Physics*, 113:9901, 11 2000. ISSN 0021-9606. doi: 10.1063/1.1329672. URL <https://aip.scitation.org/doi/abs/10.1063/1.1329672>.

- [13] B. Huang and O. A. von Lilienfeld. Ab initio machine learning in chemical compound space. *Chemical reviews*, 121(16):10001–10036, 2021.
- [14] S. Kaappa, C. Larsen, and K. W. Jacobsen. Atomic structure optimization with machine-learning enabled interpolation between chemical elements. *Physical Review Letters*, 127, 7 2021. doi: 10.1103/PhysRevLett.127.166001. URL <http://arxiv.org/abs/2107.01055><http://dx.doi.org/10.1103/PhysRevLett.127.166001>.
- [15] D. P. Kingma and J. L. Ba. Adam: A method for stochastic optimization.
- [16] A. H. Larsen, J. J. Mortensen, J. Blomqvist, I. E. Castelli, R. Christensen, M. Dułak, J. Friis, M. N. Groves, B. Hammer, C. Hargus, E. D. Hermes, P. C. Jennings, P. B. Jensen, J. Kermode, J. R. Kitchin, E. L. Kolsbjerg, J. Kubal, K. Kaasbjerg, S. Lysgaard, J. B. Maronsson, T. Maxson, T. Olsen, L. Pastewka, A. Peterson, C. Rostgaard, J. Schiøtz, O. Schütt, M. Strange, K. S. Thygesen, T. Vegge, L. Vilhelmsen, M. Walter, Z. Zeng, and K. W. Jacobsen. The atomic simulation environment—a python library for working with atoms. *Journal of Physics: Condensed Matter*, 29:273002, 6 2017. ISSN 0953-8984. doi: 10.1088/1361-648X/AA680E. URL <https://iopscience.iop.org/article/10.1088/1361-648X/aa680e><https://iopscience.iop.org/article/10.1088/1361-648X/aa680e/meta>.
- [17] X. Lu, Q. Meng, X. Wang, B. Fu, and D. H. Zhang. Rate coefficients of the $\text{h} + \text{h}_2\text{O}_2 \rightarrow \text{h}_2 + \text{HO}_2$ reaction on an accurate fundamental invariant-neural network potential energy surface. *The Journal of chemical physics*, 149(17):174303, 2018.
- [18] M. Malshe, L. Raff, M. Rockley, M. Hagan, P. M. Agrawal, and R. Komanduri. Theoretical investigation of the dissociation dynamics of vibrationally excited vinyl bromide on an ab initio potential-energy surface obtained using modified novelty sampling and feedforward neural networks. ii. numerical application of the method. *The Journal of chemical physics*, 127(13):134105, 2007.
- [19] S. Manzhos and T. Carrington Jr. Neural network potential energy surfaces for small molecules and reactions. *Chemical Reviews*, 121(16):10187–10217, 2020.
- [20] F. Neese, F. Wennmohs, U. Becker, and C. Riplinger. The orca quantum chemistry program package. *The Journal of Chemical Physics*, 152:224108, 6 2020. ISSN 0021-9606. doi: 10.1063/5.0004608. URL <https://aip.scitation.org/doi/abs/10.1063/5.0004608>.
- [21] G. D. Purvis and R. J. Bartlett. A full coupled-cluster singles and doubles model: The inclusion of disconnected triples. *The Journal of Chemical Physics*, 76:1910, 10 1998. ISSN 0021-9606. doi: 10.1063/1.443164. URL <https://aip.scitation.org/doi/abs/10.1063/1.443164>.
- [22] R. Ramakrishnan, P. O. Dral, M. Rupp, and O. A. V. Lilienfeld. Quantum chemistry structures and properties of 134 kilo molecules. *Scientific Data* 2014 1:1, 1:1–7, 8 2014. ISSN 2052-4463. doi: 10.1038/sdata.2014.22. URL <https://www.nature.com/articles/sdata201422>.
- [23] L. Ruddigkeit, R. V. Deursen, L. C. Blum, and J. L. Reymond. Enumeration of 166 billion organic small molecules in the chemical universe database gdb-17. *Journal of Chemical Information and Modeling*, 52:2864–2875, 11 2012. ISSN 15205142. doi: 10.1021/CI300415D/ASSET/IMAGES/CI-2012-00415D_M004.GIF. URL <https://pubs.acs.org/doi/full/10.1021/ci300415d>.
- [24] M. Schreiner. Transition1x. 6 2022. doi: 10.6084/m9.figshare.19614657.v4. URL <https://figshare.com/articles/dataset/Transition1x/19614657>.

- [25] K. T. Schütt, O. T. Unke, and M. Gastegger. Equivariant message passing for the prediction of tensorial properties and molecular spectra. 2021.
- [26] D. Sheppard, R. Terrell, and G. Henkelman. Optimization methods for finding minimum energy paths. *The Journal of Chemical Physics*, 128:134106, 4 2008. ISSN 0021-9606. doi: 10.1063/1.2841941. URL <https://aip.scitation.org/doi/abs/10.1063/1.2841941>.
- [27] S. Smidstrup, A. Pedersen, K. Stokbro, and H. Jónsson. Improved initial guess for minimum energy path calculations. *The Journal of Chemical Physics*, 140:214106, 6 2014. ISSN 0021-9606. doi: 10.1063/1.4878664. URL <https://aip.scitation.org/doi/abs/10.1063/1.4878664>.
- [28] J. S. Smith, B. Nebgen, N. Lubbers, O. Isayev, and A. E. Roitberg. Less is more: Sampling chemical space with active learning. *The Journal of Chemical Physics*, 148:241733, 5 2018. ISSN 0021-9606. doi: 10.1063/1.5023802. URL <https://aip.scitation.org/doi/abs/10.1063/1.5023802>.
- [29] The HDF Group. Hierarchical data format version 5, 2000-2010. URL <http://www.hdfgroup.org/HDF5>.
- [30] O. T. Unke, S. Chmiela, H. E. Sauceda, M. Gastegger, I. Poltavsky, K. T. Schutt, A. Tkatchenko, and K.-R. Muller. Machine learning force fields. *Chemical Reviews*, 121(16):10142–10186, 2021.
- [31] O. A. von Lilienfeld, K. R. Müller, and A. Tkatchenko. Exploring chemical compound space with quantum-based machine learning. *Nature Reviews Chemistry* 2020 4:7, 4:347–358, 6 2020. ISSN 2397-3358. doi: 10.1038/s41570-020-0189-9. URL <https://www.nature.com/articles/s41570-020-0189-9>.
- [32] J. Wang, S. Shin, and S. Lee. Interatomic potential model development: Finite-temperature dynamics machine learning. *Advanced Theory and Simulations*, 3:1900210, 2 2020. ISSN 2513-0390. doi: 10.1002/ADTS.201900210. URL <https://onlinelibrary.wiley.com/doi/full/10.1002/adts.201900210><https://onlinelibrary.wiley.com/doi/abs/10.1002/adts.201900210><https://onlinelibrary.wiley.com/doi/10.1002/adts.201900210>.
- [33] J. Westermayr and P. Marquetand. Machine learning for electronically excited states of molecules. *Chemical Reviews*, 121:9873–9926, 8 2021. ISSN 15206890. doi: 10.1021/ACS.CHEMREV.0C00749/ASSET/IMAGES/LARGE/CRO0C00749_0011.JPEG. URL <https://pubs.acs.org/doi/full/10.1021/acs.chemrev.0c00749>.
- [34] J. Westermayr, M. Gastegger, K. T. Schütt, and R. J. Maurer. Perspective on integrating machine learning into computational chemistry and materials science. *The Journal of Chemical Physics*, 154:230903, 6 2021. ISSN 0021-9606. doi: 10.1063/5.0047760. URL <https://aip.scitation.org/doi/abs/10.1063/5.0047760>.
- [35] T. A. Young, T. Johnston-Wood, V. L. Deringer, and F. Duarte. A transferable active-learning strategy for reactive molecular force fields. *Chemical science*, 12(32):10944–10955, 2021.
- [36] P. M. Zimmerman. Single-ended transition state finding with the growing string method. *Journal of Computational Chemistry*, 36:601–611, 4 2015. ISSN 1096-987X. doi: 10.1002/JCC.23833. URL <https://onlinelibrary.wiley.com/doi/full/10.1002/jcc.23833><https://onlinelibrary.wiley.com/doi/abs/10.1002/jcc.23833><https://onlinelibrary.wiley.com/doi/10.1002/jcc.23833>.